

# Electronic Supporting Information

for

## Isotope effect analyses provide evidence for an altered transition state for RNA 2'-*O*-transphosphorylation catalyzed by Zn<sup>2+</sup>

Shuming Zhang, Hong Gu, Emily Strong, Edward W. Ollie, Daniel Kellerman, Haoyuan Chen, Danni Liang, Vernon E. Anderson, Joseph A. Piccirilli, Darrin M. York and Michael E. Harris

### Contents

1. Non-enzymatic catalysis of RNA 2'-*O*-transphosphorylation by Zn<sup>2+</sup>.
2. Zn<sup>2+</sup> concentration dependence of  $k_{\text{obs}}$ .
3. Solvent D<sub>2</sub>O effect measurement and proton inventory analyses.
4. Determination of primary and secondary <sup>18</sup>O kinetic isotope effects.

**Table S1.** Nucleophile (<sup>18</sup> $k_{\text{NUC}}$ ), leaving group (<sup>18</sup> $k_{\text{LG}}$ ), and non-bridging oxygen (<sup>18</sup> $k_{\text{NPO}}$ ) KIEs on intramolecular transphosphorylation and hydrolysis reactions.

**Figure S1.** Non-enzymatic Zn<sup>2+</sup> catalysis of 2'-*O*-transphosphorylation of the dinucleotide 5'-UpG-3'.

**Figure S2.** Analysis of the Zn<sup>2+</sup> concentration dependence of  $k_{\text{obs}}$  for UpG 2'-*O*-transphosphorylation.

**Figure S3.** Analysis of the pH dependence of  $k_{\text{obs}}$  for RNA 2'-*O*-transphosphorylation catalyzed by Zn<sup>2+</sup>.

## Methods and Supplementary Data

### 1. Non-enzymatic catalysis of RNA 2'-O-transphosphorylation by Zn<sup>2+</sup>.

Reaction conditions for D<sub>2</sub>O solvent kinetic isotope effect (SKIE) and <sup>18</sup>O primary and secondary kinetic isotope effect (KIE) measurements were selected to correspond as closely as possible to previous physical and chemical analyses, in particular linear free energy relationship analyses of Zn<sup>2+</sup> catalysis of RNA model transphosphorylation reactions and previous mechanistic studies<sup>1-6</sup>. Unless otherwise noted RNA 2'-O-transphosphorylation reactions contained 20 - 50 μM of the substrate dinucleotide uridylyl-3',5'-guanosine (5'-UpG-3'), Zn(NO<sub>3</sub>)<sub>2</sub> (at the concentrations indicated in the text), 0.1 M NaNO<sub>3</sub> and 0.02 M HEPES (pH 7.0 or as indicated) at 90°C. Aliquots were taken at specific times and frozen or temporarily placed on ice. The conversion of precursor to products was quantified by reverse phase HPLC as described previously<sup>7, 8</sup> (**Figure S1**). Briefly, a KLB Bromma 2150 HPLC pump was used with detection at 260 nm using a Shimadzu SPD-6AV UV-Vis detector coupled to a C18 column (300 x 3.9 mm, 10 μm; Phenomenex) run isocratically at 1 ml/min using a mobile phase of 0.1 M ammonium acetate containing 4% acetonitrile. Peaks were identified using standards and analyses of UV absorbance and their areas were recorded and quantified using a SP4290 integrator (Spectra Physics, USA). The fraction of the unreacted UpG substrate ( $F = [\text{UpG}] / [\text{UpG}]_0$ ) was calculated according to  $F = A_{\text{UpG}} / [A_{\text{UpG}} + A_G + A_{2',3'\text{-cUMP}} + \text{hydrolyzed isomers}]$ , where  $A_{\text{UpG}}$  is the area of the UpG peak,  $A_G$  is the peak area for guanosine and  $A_{2',3'\text{-cUMP}} + \text{hydrolyzed isomers}$  are the combined areas of 2',3'-cUMP and the uridine-2'-monophosphate (U-2'-P) and uridine-3'-monophosphate (U-3'-P) secondary hydrolysis products (**Figure S1**).

Heavy atom oxygen KIEs were determined by analyzing the change in isotope ratio (<sup>18</sup>O/<sup>16</sup>O) in the residual substrate. Therefore, the isotopic fractionation only reports on the rate limiting 2'-O-transesterification reaction and is unaffected by subsequent reactions involving the 2',3'-cUMP product. Under these reaction conditions a product that would be consistent with migration of 2',5'-UpG, which is readily observed in the reaction catalyzed by acid<sup>9, 10</sup>, was not observed to form in the Zn<sup>2+</sup>-catalyzed reaction. This data is consistent with previous results showing preferential catalysis of transphosphorylation over isomerization, which is consistent with Zn<sup>2+</sup> stabilization of an anionic TS similar to the specific base reaction<sup>2, 11, 12</sup>.

The time dependent conversion of substrate to product for non-enzymatic catalysis by both specific base and by Zn<sup>2+</sup> aquo ions follow first order kinetics and proceed. The observed first order rate constant ( $k_{\text{obs}}$ ) were measured by fitting to,

$$F = F_T e^{-k_{\text{obs}}t} + F_0 \quad (\text{Eq. 1}),$$

where  $F_T$  and  $F_0$  are the amplitude and initial values, respectively. The  $k_{\text{obs}}$  values reported for the analyses of pH, Zn<sup>2+</sup> concentration dependence and solvent D<sub>2</sub>O effects are reported as the average and standard deviation calculated from at least three independent trials. Standard errors in the last digit are shown in parenthesis for the KIEs in the text and in **Table S1**.

## 2. Zn<sup>2+</sup> concentration dependence of $k_{\text{obs}}$

Non-enzymatic intramolecular transphosphorylation reactions catalyzed by Zn<sup>2+</sup> ions and organometallic Zn<sup>2+</sup> complexes in solution have been highly informative model systems for understanding the roles of divalent metal ions in phosphoryl transfer catalysis<sup>11-14</sup>. Compared to Mg<sup>2+</sup>, which is more common in phosphodiesterase active sites, Zn<sup>2+</sup> differs in absolute hardness (47.6 versus 10.9). However, it has similar coordination geometry (6), ionic radius (0.72 versus 0.74 Å) and absolute electronegativity (28.2 versus 32.5)<sup>15</sup>. Although it is found less frequently than Mg<sup>2+</sup>, Zn<sup>2+</sup> also functions in the active sites of numerous enzymes including phosphoryl transferases<sup>16</sup>, and thus a detailed examination of its mechanism is likely to be broadly applicable to other divalent ions.

The observed rate constant for transphosphorylation at pH 7.0, 0.1 M NaNO<sub>3</sub> is dependent on Zn<sup>2+</sup> concentration, but shows downward curvature at higher concentrations (**Figure S2**). Interpretation of these data with respect to the affinity and number of metal ions interacting with the TS is complicated by the limited range of concentrations and conditions available due to solubility, as well as the potential for inhibitory complexes to form between Zn<sup>2+</sup> and the substrate nucleobases<sup>17</sup>. However, the observed concentration dependence places constraints on the possible number and affinity of catalytic ions. Plotted on a log-log scale both concentration dependent and concentration independent phases are observed. This behavior is consistent with mechanisms involving association of metal ion(s) prior to formation of the rate limiting TS as illustrated in **Scheme 1**<sup>18, 19</sup>.

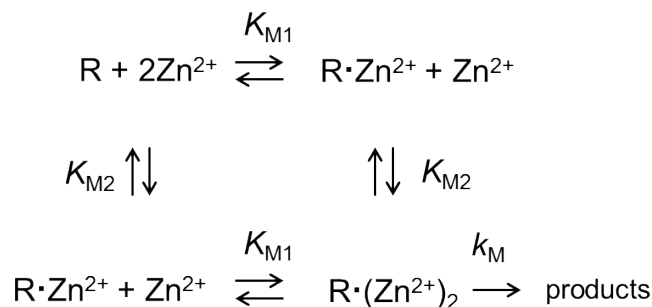


**Scheme 1**

In this model  $K_M$  is the equilibrium constant for formation of ground state complexes between the RNA and metal ion and  $k_M$  is the intrinsic rate constant for reaction of preformed complexes to form product. The data for  $k_{obs}$  versus  $[Zn^{2+}]$  were analyzed using the mechanism in **Scheme 1** by fitting to a single-site saturation binding equation,

$$k_{obs} = \frac{k_M}{(1 + K_M/[Zn^{2+}])} + k_{OH} \quad (\text{Eq. 2}),$$

in which  $k_M$  is the intrinsic rate constant for the reaction of the RNA-metal ion complex,  $K_M$  is the apparent dissociation constant for the complex and  $k_{OH}$  is the observed rate constant in the absence of  $Zn^{2+}$ . However, the data are not well described by this simple mechanism as indicated by  $R^2$  values of  $<0.6$ , therefore, more complex mechanisms may be considered.



**Scheme 2**

A general two metal ion mechanism is illustrated in **Scheme 2** in which  $K_{M1}$  and  $K_{M2}$  are the binding constants for two  $Zn^{2+}$  ions. Within this mechanism it is possible that the observed rate constant for product formation is the result of a mixture of one- and two-metal ion reaction channels, as observed for  $Ca^{2+}$  catalysis of phosphodiester hydrolysis<sup>18</sup>. However, such a mixed mechanism predicts that the  $Zn^{2+}$  dependence of  $k_{obs}$  would follow a quadratic function at low concentrations and show apparent saturation (hyperbolic behavior) at higher concentrations<sup>18, 20</sup>, which is not observed. However, the data can be described using a cooperative binding model,

$$k_{obs} = \frac{k_M}{(1 + K_M/[Zn^{2+}]^2)} + k_{OH} \quad (\text{Eq. 3}).$$

As shown in **Figure S2** the observed  $\text{Zn}^{2+}$  dependence of  $k_{\text{obs}}$  fits this model with an  $n$  value of 2, which is consistent with mechanisms that involve the binding of two or more  $\text{Zn}^{2+}$  ions<sup>20</sup>.

The apparent saturation at high concentrations of  $\text{Zn}^{2+}$  is consistent with formation of ground state complexes between the metal ion and RNA. However, it must be noted that formation of inhibitory or poorly active complexes between  $\text{Zn}^{2+}$  in organometallic compounds in the catalysis of RNA model reactions has been observed<sup>17, 21, 22</sup>. Such inhibitory complexes effects could formally account for, or contribute to the observed saturation behavior and apparent cooperativity. There are two main factors that suggest this is unlikely to be the case for  $\text{Zn}^{2+}$  catalysis of 2'-*O*-transphosphorylation of the dinucleotide UpG. First, the nucleobase specificity of  $\text{Zn}^{2+}$  catalysis of RNA strand cleavage is relatively low. In the literature the dinucleotide UpU shows the largest rate increase in  $\text{Zn}^{2+}$  compared to the other three homodinucleotides although the differences are less than ten-fold<sup>23</sup>. Second, the pH dependence of UpG 2'-*O*-transphosphorylation catalyzed by  $\text{Zn}^{2+}$  is inconsistent with inhibitory metal interactions with the N3 of the uridine nucleobase observed with some  $\text{Zn}^{2+}$  organometallic catalysts. Formation of this interaction requires deprotonation of the nucleobase and therefore greater inhibition should be observed as pH increases<sup>17</sup>, which is not consistent with the data. Mechanistic experiments were nonetheless performed at low (10 mM)  $\text{Zn}^{2+}$  concentration to permit comparison of the differences in bonding between the TS and the free, unbound RNA phosphoryl group in solution.

### 3. Solvent D<sub>2</sub>O effect measurement and proton inventory analyses.

The observed rate constant for  $\text{Zn}^{2+}$  catalysis of UpG transphosphorylation is log-linearly dependent on hydroxide concentration (**Figure S3A**) as previously reported for  $\text{Zn}^{2+}$  catalysis of uridine 3'-*p*-nitrophenol phosphate reactions<sup>14, 23</sup>. Due to the formation of insoluble Zn-hydroxide complexes, the analysis of pH dependence is restricted to values below *ca.* pH 7.0. However, under these conditions the  $k_{\text{obs}}$  in the absence of  $\text{Zn}^{2+}$  is slow ( $< 0.0001 \text{ min}^{-1}$ ) and is nearly independent of pH due to reaction via both acid and base catalyzed reaction channels<sup>9</sup>. The significant increase in rate constant at millimolar concentrations of  $\text{Zn}^{2+}$  allows the effects of metal ion catalysis on transition state structure to be isolated and characterized independent of the background uncatalyzed reaction (**Figure S2**).

The amount of rate enhancement of UpG 2'-*O*-transphosphorylation provided by  $\text{Zn}^{2+}$  referred to in the text is estimated by comparing the second order rate constants for hydroxide ion dependence in the presence and absence of the divalent metal ion catalyst. The second order rate constant with respect to hydroxide concentration was measured for UpG cleavage at pH  $> 9$  yielding a value of  $4.5 \text{ M}^{-1}\text{min}^{-1}$  as reported previously<sup>7</sup>. This value increases to *ca.*  $5 \times 10^4 \text{ M}^{-1}\text{min}^{-1}$  in the presence of 10 mM  $\text{Zn}^{2+}$

measured at pH values  $< 7$ . Assuming that the linear dependence on hydroxide concentration observed for the specific base reaction extrapolates to the neutral pH range then the rate enhancement provided by  $\text{Zn}^{2+}$  is *ca.* 12,000-fold. These results are consistent with previous reports of  $\text{Zn}^{2+}$ -catalyzed cleavage of polyU showing *ca.* 2000-fold rate enhancement and *ca.* 500-fold catalysis of thymidine *p*-nitrophenol hydrolysis by  $\text{Mg}^{2+}$  ions<sup>18,24</sup>.

As stated in the text, the pH dependence together with lack of isomerization products suggests that  $\text{Zn}^{2+}$  stabilizes an anionic TS similar to the specific base mechanism. However, limitations due to kinetic ambiguity do not allow the alternative proton transfer mechanisms (general or specific base) to be distinguished by these data alone. For specific base catalysis of RNA 2'-*O*-transphosphorylation an apparent  $\text{p}K_a$  is observed in pH-log  $k$  profiles at *ca.* pH 13 that reflects equilibrium deprotonation of the 2'-O to form an oxyanion<sup>7</sup>. The simplest model for the  $\text{Zn}^{2+}$ -catalyzed reaction is a similar specific base mechanism with involving equilibrium deprotonation of the 2'OH that is defined by the equilibrium constant  $K_{\text{OH}}$ , and involves an anionic transition state ( $\text{TS}_{\text{SB}}$ ) (**Figure S3B**). In this mechanism, the log-linear dependence of  $k_{\text{obs}}$  reflects the increase in the reactive 2'O oxyanion species in the ground state. A kinetically equivalent general base mechanism involves a  $\text{Zn}^{2+}$  coordinated hydroxide ion acting as an H acceptor, in which loss of the 2'O proton occurs in the transition state ( $\text{TS}_{\text{GB}}$ ). For this mechanism, the pH dependence reflects increase in the concentration of the metal hydroxide catalyst defined by the equilibrium constant  $K_{\text{M(OH)}}$ .

As described in the text solvent SKIE analyses were pursued to gain additional insight into the issue of proton transfer mechanism. The solvent  $\text{D}_2\text{O}$  effect on 2'-*O*-transphosphorylation of UpG catalyzed with  $\text{Zn}^{2+}$  ion reported in the text and shown in **Figure 2** were determined by measuring the  $k_{\text{obs}}$  as described above using solution stocks prepared with  $\text{D}_2\text{O}$  except for concentrated substrate stocks which were prepared in  $\text{H}_2\text{O}$  and contributed  $< 5\%$  to the total reaction volume. This level of systematic error is outside of the experimental error in measurements of  $k_{\text{obs}}$  and the reported values are not corrected for the small amount of contaminating  $\text{H}_2\text{O}$  in the reaction. The 0.1 M stocks of HEPES at a pL of 7.0 were prepared at  $25^\circ\text{C}$  assuming a  $\Delta\text{p}K_a/^\circ\text{C}$  of  $-0.014^{25}$  using a  $+0.4$  correction of the pH meter reading for the  $\text{D}_2\text{O}$  sample<sup>26</sup>. The difference in the temperature dependences of the ionization constants for  $\text{H}_2\text{O}$  and  $\text{D}_2\text{O}$  necessarily gives rise to a small difference in the pH of the two solutions at the higher reaction temperature. Based on potentiometric studies the dependences are  $-0.0344 \Delta\text{p}K_a/^\circ\text{C}$  for  $\text{D}_2\text{O}$  versus  $-0.0325 \Delta\text{p}K_a/^\circ\text{C}$  for  $\text{H}_2\text{O}^{27}$ , resulting in at most a 0.07 pH unit difference between the two solutions. This difference would potentially give rise to a 17% underestimate of the effect of complete substitution of  $\text{H}_2\text{O}$  by  $\text{D}_2\text{O}$  on the  $k_{\text{obs}}$  which is within the range of experimental error for individual measurements. The

values for  $k_{\text{H}}/k_{\text{D}}$  reported in the text represent the average of at least five independent experiments. Proton inventory analyses were performed by determining  $k_{\text{obs}}$  as a function of the mole fraction of  $\text{D}_2\text{O}$ . Reactions were performed by mixing reactions containing only  $\text{H}_2\text{O}$  and  $\text{D}_2\text{O}$  in proportions to achieve the desired ratio of solvent ranging from  $n=0$  to  $n=1$  in twenty percent increments. The rate constants analyzed in **Figure 2** are averages from at least three independent experiments performed in this manner. The proton inventory data were fit to the Gross-Butler equation for multiple H/D fractionation factors according to,

$$k_n = k_0 \frac{\prod (1 - n + n\varphi^{\text{T}})}{\prod (1 - n + n\varphi^{\text{R}})} \quad (\text{Eq. 3})$$

where  $k_n$  is the observed rate constant at  $\text{D}_2\text{O}$  mole fraction of  $n$ ,  $k_0$  is the rate constant in  $\text{H}_2\text{O}$  and  $\varphi^{\text{R}}$  and  $\varphi^{\text{T}}$  are fractionation factors in the reactant (ground) state and transition state, respectively. The proton inventory data were fit or simulated using **Eq. 3** using the values for the  $\varphi^{\text{R}}$  and  $\varphi^{\text{T}}$  fractionation factors as described in the text and the legend for **Figure 2**.

#### 4. Determination of primary and secondary $^{18}\text{O}$ kinetic isotope effects.

Kinetic isotope effects were measured using the internal competition method<sup>28, 29</sup> in which the change in the ratio of  $^{16}\text{O}/^{18}\text{O}$  in the residual UpG substrate is quantitatively analyzed as a function of reaction progress<sup>7, 8</sup>. Briefly, RNA molecules were synthesized in which the 2' O, 5' O or one of the non-bridging oxygens was enriched in  $^{18}\text{O}$  as previously described. Note that the incorporation of  $^{18}\text{O}$  into the non-bridging oxygen position, which is accomplished using  $\text{H}_2^{18}\text{O}$  in the oxidation step of solid phase synthesis from phosphoramidite monomers, is random. As a consequence the observed  $^{18}k_{\text{NPO}}$  reported in **Figure 3** is an average of the effects at the two positions. The interpretation of these data assumes that the changes in the bonding environments of the two non-bridging oxygens in the transition state are similar at both positions. Thus, it is assumed that the observed  $^{18}k_{\text{NPO}}$  can be interpreted without accounting for the potential for significantly different KIEs at the two positions. The model interpretations discussed in the text are based on the total collection of observed KIE and SKIE data, and therefore do not rely on any initial assumptions regarding the stereospecificity of  $^{18}k_{\text{NPO}}$  effects.

To determine KIEs mixtures of  $^{18}\text{O}$  and  $^{16}\text{O}$  containing RNA were used in reactions catalyzed by either hydroxide or  $\text{Zn}^{2+}$ , as described, above. The residual, unreacted UpG substrate was purified using RP-HPLC from time points taken over the course of the reaction and the  $^{16}\text{O}/^{18}\text{O}$  ratio determined by

whole molecule mass spectrometry as outlined, below, and as described in more detail previously<sup>7, 30</sup>. The synthesis of Up[NPO-<sup>18</sup>O]G, Up[2'-<sup>18</sup>O]G, and Up[5'-<sup>18</sup>O]G were described previously<sup>32,33</sup>. The isotope <sup>18</sup>O-labeled and unlabeled UpG were combined in approximately 1:1 ratios at least 5 samples were collected at different reacted time points (5 to 95% reaction). The purified, unreacted UpG was dried under vacuum and further lyophilized 3-4 additional times after resuspending in 1mL water. The recovered material was dissolved in H<sub>2</sub>O-acetonitrile (1:1, v/v) and the <sup>16</sup>O/<sup>18</sup>O ratios were quantified by electrospray ionization quadrupole/time of flight tandem mass spectrometry (ESI-Q/TOF MS/MS) (ABI QSTAR) in negative ion mode using direct infusion. The entire isotopic cluster of the unlabeled and <sup>18</sup>O-labeled (M – H)<sup>-</sup> ions of UpG (*m/z* 588 and 590, respectively) was isolated in the quadrupole mass analyzer and fragmented with a collision energy of 35 eV. The tandem mass spectra were acquired by the TOF analyzer for 10-15 min with scan speed of 1 sec per scan. Two product ion pairs containing the isotopically labeled oxygen, *m/z* 476/478 and 211/213, were used to calculate the <sup>16</sup>O/<sup>18</sup>O ratios by integrating the peaks assuming uniform Gaussian shapes using Origin; however, the data often achieved sufficient baseline separation to allow the integrated values to be obtained directly using the Analyst software. As illustrated in **Figure S4** the resulting data are fit to,

$$\ln(R_s) = (1/^{18}k - 1)\ln(1 - F) + \ln(R_0) \quad (\text{Eq. 4})$$

where <sup>18</sup>*k* is the isotope effect, *F* is the fraction of unreacted (residual) substrate (UpG) quantified by RP-HPLC, and *R<sub>s</sub>* and *R<sub>0</sub>* are the ratios of <sup>16</sup>O/<sup>18</sup>O for the unreacted substrate at *F* and its initial value, respectively.

**Table S1. Nucleophile ( $^{18}k_{\text{NUC}}$ ), leaving group ( $^{18}k_{\text{LG}}$ ), and non-bridging oxygen ( $^{18}k_{\text{NPO}}$ ) KIEs on intramolecular transphosphorylation and hydrolysis reactions.**

Substrate	$^{18}k_{\text{NUC}}$	$^{18}k_{\text{LG}}$	$^{18}k_{\text{NPO}}$	reference
<b>Uridyl-3',5'-guanosine (UpG)</b>				
RNase A, 0.1M NaCl, pH 7, 37°C	0.994(2)	1.014(3)	1.001(1)	8
pH 14, 37°C	0.984(3)	1.034(4)	-	7
pH 0, 37°C	0.990(4)	1.005(4)	0.991(1)	8
pH 12, 1 M NaCl, 37°C	0.996(2)	1.037(2)	0.999(1)	7, 30
pH 12, 0.1 M NaNO <sub>3</sub> , 90°C	0.997(1)	1.034(3)	-	this study
10 mM ZnNO <sub>3</sub> , pH 7, 0.1 M NaNO <sub>3</sub> , 90°C	0.986(4)	1.015(2)	1.0007(2)	this study
<b>U-3'-m-nitrobenzyl phosphate<sup>a</sup></b>				
pH 10, 27°C	-	1.0272(1)	-	31
pH 2.5, 27°C	-	1.0019(7)	0.9904	31
pH 5.5, 27°C	-	1.009(1)	0.9990	31
<b>U-3'-p-nitrophenol phosphate<sup>b</sup></b>				
specific base	-	1.0059 (9)	-	32
acid catalysis	-	1.006 (1)	-	32
<b>hydroxypropyl-p-nitrophenol phosphate</b>				
specific base	1.0327(8) <sup>c</sup>	1.0064(9)	-	5
diZn compound L(OH) <sub>2</sub> <sup>a</sup>	1.0116(10)	1.0113(5)	-	5
<b>thymidine 3'-p-nitrophenol phosphate</b>				
specific base	1.068(7) <sup>d</sup>	-	-	33
1 M NaCl, 25 mM Mg <sup>2+</sup>	1.027(1)	-	-	34
<b>p-tert-butylphenyl-p-nitrophenol phosphate</b>				
specific base	-	1.0046(8)	1.0040(1)	35
specific acid	-	1.0058(5)	0.9926(2)	35
<b>3,3-dimethylbutyl-p-nitrophenol phosphate</b>				
specific base	-	1.0059(5)	0.9949(6)	35
specific acid	-	1.0036(4)	1.0139(4)	35
<b>ethyl p-nitrophenyl phosphate</b>				
10 mM Co(III) cyclen pH 7, 50°C	-	1.022 (1)	0.9948 (5)	36
40 mM Zn(II) cyclen, pH 8.5, 80 °C	-	1.0095 (1)	1.0108 (5)	36
10mM Eu(III), pH 6.3, 50 °C	-	1.016 (1)	1.0016 (7)	36

<sup>a</sup>The  $pK_a$  of *m*-nitrobenzyl is *ca.* 13 and therefore is similar to the unreactive 5'O leaving group of RNA as compared to the lower  $pK_a$  of the more reactive nitrophenol leaving group. The transition state is highly sensitive to leaving group charge accumulation as demonstrated by linear free energy relationship data as well as the KIE results shown here<sup>37</sup>.

<sup>b</sup>The analysis of the leaving group KIEs for *p*-nitrophenol phosphodiester determined by Cleland, Hengge and colleagues were accompanied by analysis of the secondary KIE on the N atom of the nitro group<sup>29, 38</sup>. Delocalization of negative charge from the leaving group oxygen onto the ring results in a normal secondary KIE at this position allowing this aspect of mechanism to be more clearly revealed. To a first approximation the magnitude of the effects on *p*-nitrophenol leaving group can be compared in the absence of this effect, and for clarity it is omitted since there is no directly analogous KIE for RNA.

<sup>c</sup>L(OH)<sub>2</sub> is a dinuclear Zn compound developed and characterized by the Morrow and Richards<sup>14</sup>. Solvent D<sub>2</sub>O and pH dependence support a proposed mechanism involving base catalysis as well as electrostatic stabilization.

<sup>d</sup>Nucleophile KIEs contain contributions from deprotonation and the kinetic effect on nucleophilic attack<sup>5,7</sup>. The kinetic effect itself contains contributions from a temperature-independent factor (TIF) and the temperature-dependent factor (TDF). The TIF reflects the extent to which the labeled atom participates in reaction coordinate motion and always favors the lighter isotope since its imaginary frequency, the new vibrational mode formed in the transition state, is larger. The TDF reflects all the other differences in bond vibrations involving the labeled atom between the ground state compared and transition state. As a consequence nucleophile KIEs are generally normal when nucleophile bond formation occurs in the rate-limiting step are largest for early transition states. Values decrease as bonding to the nucleophile in the transition state increases and inverse nucleophile KIEs such as those observed for RNA are observed for late transition states due to advanced bond formation.

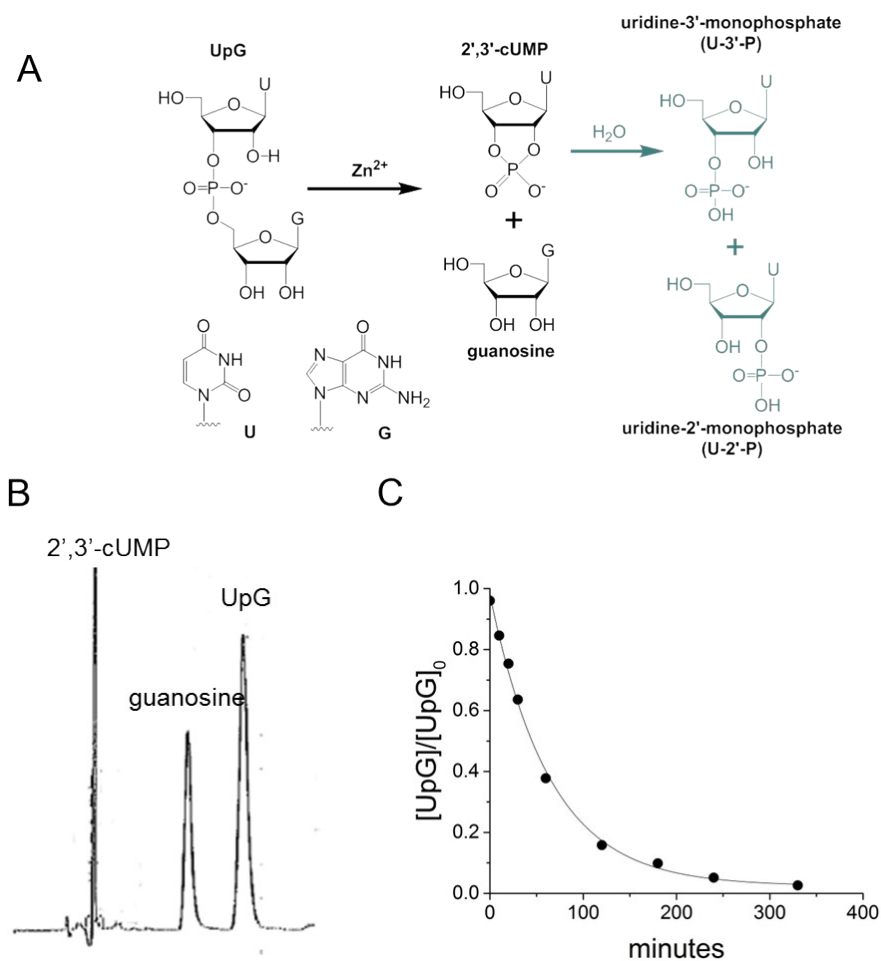


**Figure S1.** Non-enzymatic  $\text{Zn}^{2+}$  catalysis of 2'-*O*-transphosphorylation of the dinucleotide 5'-UpG-3'. **A.** Reactant dinucleotide UpG reacts via 2'-*O*-transphosphorylation to form 2',3'-cUMP and guanosine. The cUMP is then hydrolyzed to generate a mixture of uridine-2'-monophosphate (U-2'-P) and uridine-3'-monophosphate (U-3'-P). KIE measurements were conducted using internal competition analysis of the change in isotope rate in the residual UpG and therefore are unaffected by further reaction of the products. **B.** Separation and quantification by RP-HPLC as described. The peaks corresponding to the reactants and products are indicated. The UMP peak contains both the initial cUMP as well as subsequent hydrolysis products. **C.** The data for the conversion of UpG obtained by integration of the HPLC chromatograms to Eq. 1 to determine the observed rate constant ( $k_{\text{obs}}$ ).

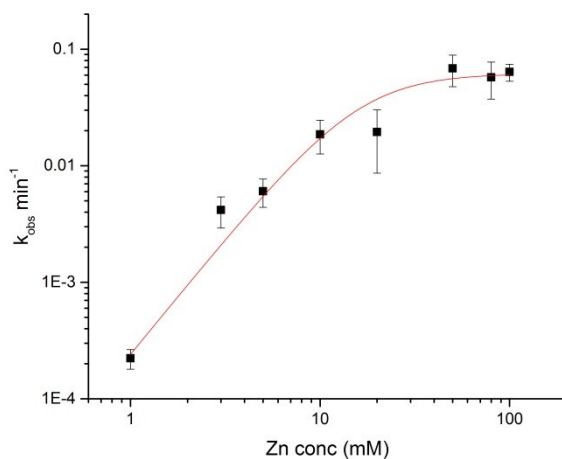


**Figure S2.** Analysis of the  $\text{Zn}^{2+}$  concentration dependence of UpG 2'-*O*-transphosphorylation in 40 mM HEPES pH 7.0, 0-0.1M  $\text{NaNO}_3$  to maintain constant  $I$ . Curvature in concentration dependence suggests saturation behavior consistent with catalytic complexes between  $\text{Zn}^{2+}$  and UpG. The line shows a fit of the data to a model for formation of ground state complexes between UpG and  $\text{Zn}^{2+}$  involving two ions as described by **Scheme 2** and **Eq. 3**.

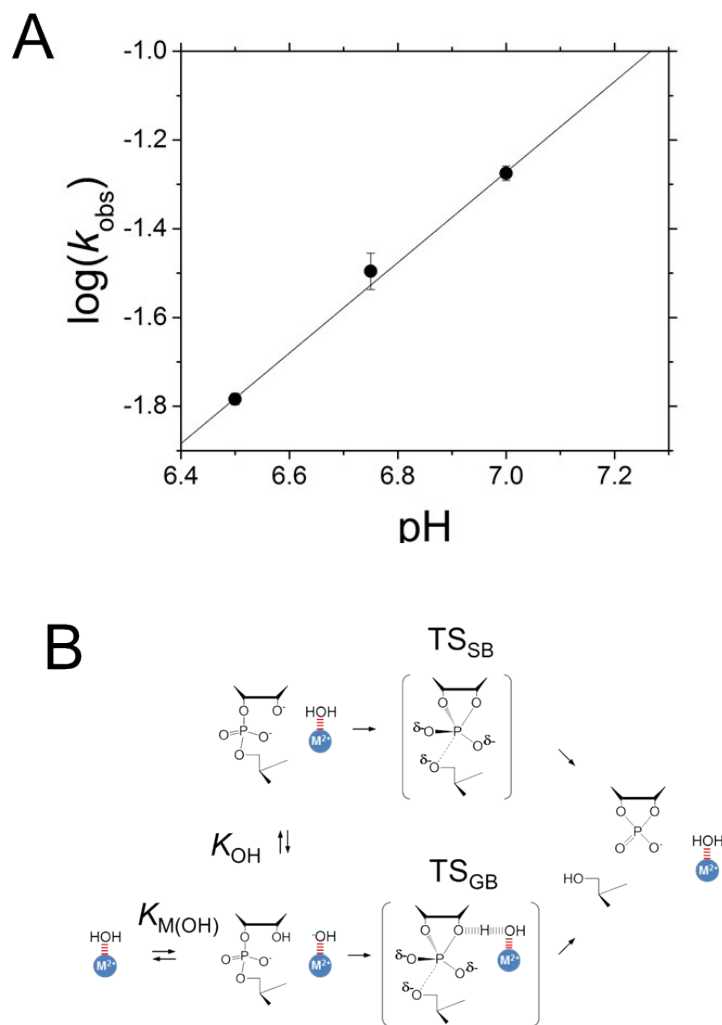


**Figure S3.** Analysis of the pH dependence of  $k_{\text{obs}}$  for RNA 2'-*O*-transphosphorylation catalyzed by  $\text{Zn}^{2+}$ . **A.** Plot of  $\log(k_{\text{obs}})$  versus reaction pH under conditions of 10 mM  $\text{Zn}(\text{NO}_3)_2$ , 0.1M  $\text{NaNO}_3$ , 20 mM HEPES at pH values indicated. **B.** General and Specific Base mechanisms of 2'O nucleophile activation by  $\text{Zn}^{2+}$  coordinated hydroxide. In the Specific Base mechanism (top pathway) the 2'O proton is transferred in a pre-equilibrium step with equilibrium constant  $K_{\text{OH}}$  followed by nucleophilic attack and formation of the rate limiting  $\text{TS}_{\text{SB}}$ . In the General Base mechanism (bottom pathway) the 2'O proton is transferred to the metal hydroxide catalyst as part of  $\text{TS}_{\text{GB}}$ . In both mechanisms the equilibrium constant for formation of the metal hydroxide catalyst is  $K_{\text{M}(\text{OH})}$ .

## Supplemental References

1. S. Mikkola, E. Stenman, K. Nurmi, E. Yousefi-Salakdeh, R. Stromberg and H. Lonnberg, *J. Chem. Soc., Perkin Trans*, 1999, **2**, 1619-1625.
2. H. Korhonen, T. Koivusalo, S. Toivola and S. Mikkola, *Org Biomol Chem*, 2013, **11**, 8324-8339.
3. M. Y. Yang, O. Iranzo, J. P. Richard and J. R. Morrow, *J Am Chem Soc*, 2005, **127**, 1064-1065.
4. R. A. Mathews, C. S. Rossiter, J. R. Morrow and J. P. Richard, *Dalton Trans*, 2007, 3804-3811.
5. T. Humphry, S. Iyer, O. Iranzo, J. R. Morrow, J. P. Richard, P. Paneth and A. C. Hengge, *J Am Chem Soc*, 2008, **130**, 17858-17866.
6. R. Breslow and D. L. Huang, *Proc Natl Acad Sci U S A*, 1991, **88**, 4080-4083.
7. M. E. Harris, Q. Dai, H. Gu, D. L. Kellerman, J. A. Piccirilli and V. E. Anderson, *J Am Chem Soc*, 2010, **132**, 11613-11621.
8. H. Gu, S. Zhang, K. Y. Wong, B. K. Radak, T. Dissanayake, D. L. Kellerman, Q. Dai, M. Miyagi, V. E. Anderson, D. M. York, J. A. Piccirilli and M. E. Harris, *Proc Natl Acad Sci U S A*, 2013, **110**, 13002-13007.
9. M. Oivanen, S. Kuusela and H. Lonnberg, *Chemical Rev*, 1998, **98**, 961-990.
10. M. Kosonen, E. Yousefi-Salakdeh, R. Stromberg and H. Lonnberg, *J. Chem. Soc., Perkin Trans*, 1998, 1589-1595.
11. H. Korhonen, N. H. Williams and S. Mikkola, *J Phys Org Chem*, 2013, **26**, 182-186.
12. D. L. Kellerman, D. M. York, J. A. Piccirilli and M. E. Harris, *Curr Op Chem Biol*, 2014, **21c**, 96-102.
13. H. Lonnberg, *Org Biomolec Chem*, 2011, **9**, 1687-1703.
14. J. R. Morrow, T. L. Amyes and J. P. Richard, *Acc Chem Res*, 2008, **41**, 539-548.
15. D. T. Richens, *The Chemistry of Aqua Ions: Synthesis, Structure and Reactivity: A Tour Through the Periodic Table of the Elements*, Wiley, 1997.
16. K. A. McCall, C. Huang and C. A. Fierke, *J Nutrition*, 2000, **130**, 1437S-1446S.
17. C. S. Rossiter, R. A. Mathews and J. R. Morrow, *Inorg Chem*, 2005, **44**, 9397-9404.
18. B. A. Kirk, C. L. Cusack, E. Laager, E. Rochlis, T. Thomas and A. G. Cassano, *J Inorg Biochem*, 2010, **104**, 207-210.
19. D. Herschlag and W. P. Jencks, *Biochemistry*, 1990, **29**, 5172-5179.
20. A. Fersht, *Structure and Mechanism in Protein Science*, W.H. Freeman & Co., 1998.
21. C. S. Rossiter, R. A. Mathews, I. M. del Mundo and J. R. Morrow, *J Inorg Biochem*, 2009, **103**, 64-71.
22. M. F. Mohamed, I. Sanchez-Lombardo, A. A. Neverov and R. S. Brown, *Org Biomol Chem*, 2012, **10**, 631-639.
23. H. Ikenaga and Y. Inoue, *Biochemistry*, 1974, **13**, 577-582.
24. R. Breslow, D. L. Huang and E. Anslyn, *Proc Natl Acad Sci U S A*, 1989, **86**, 1746-1750.
25. N. E. Good, G. D. Winget, W. Winter, T. N. Connolly, S. Izawa and R. M. M. Singh, *Biochemistry*, 1966, **5**, 467-477.
26. D. M. Chadalavada, A. L. Cerrone-Szakai, J. L. Wilcox, N. A. Siegfried and P. C. Bevilacqua, *Methods Mol Biol*, 2012, **848**, 21-40.
27. A. K. Covington, R. A. Robinson and R. G. Bates, *Journal Phys Chem*, 1966, **70**, 3820-3824.
28. J. Bigeleisen and M. Wolfsberg, *Adv. Chem. Phys.*, 1958, **1**, 15-76.
29. W. W. Cleland, *Arch Biochem Biophys*, 2005, **433**, 2-12.
30. K. Y. Wong, H. Gu, S. Zhang, J. A. Piccirilli, M. E. Harris and D. M. York, *Angew Chem Int Ed Engl*, 2012, **51**, 647-651.
31. B. Gerratana, G. A. Sowa and W. W. Cleland, *J Am Chem Soc*, 2000, **122**, 12615-12621.

32. A. C. Hengge, K. S. Bruzik, A. E. Tobin, W. W. Cleland and M. D. Tsai, *Bio-Organic Chemistry*, 2000, **28**, 119-133.
33. A. G. Cassano, V. E. Anderson and M. E. Harris, *J Am Chem Soc*, 2002, **124**, 10964-10965.
34. A. G. Cassano, V. E. Anderson and M. E. Harris, *Biochemistry.*, 2004, **43**, 10547-10559.
35. A. C. Hengge and W. W. Cleland, *FASEB Journal*, 1991, **113**, 5835-5841.
36. J. Rawlings, W. W. Cleland and A. C. Hengge, *J Am Chem Soc*, 2006, **128**, 17120-17125.
37. H. Chen, T. J. Giese, M. Huang, K. Y. Wong, M. E. Harris and D. M. York, *Chemistry-A European Journal*, 2014, **20**(44):14336-43.
38. W. W. Cleland and A. C. Hengge, *Chem Rev*, 2006, **106**, 3252-3278.